



# Forward Proton ID Certification I: Elastic Process and Standalone DAQ

G.A. Alves,<sup>1</sup> C. Avila,<sup>4</sup> J. Barreto,<sup>1,†</sup> V. Bodyagin,<sup>6</sup> A. Brandt,<sup>8</sup> W. Carvalho,<sup>2</sup>  
E.M. Gregores,<sup>3</sup> P. Hanlet,<sup>8</sup> M. Martens,<sup>7</sup> J. Molina,<sup>1</sup> J. Montanha,<sup>1</sup>  
H. da Motta,<sup>1</sup> S.F. Novaes,<sup>3</sup> V. Oguri,<sup>2</sup> N. Oliveira,<sup>1</sup> C. de Oliveira Martins,<sup>2</sup>  
W.L. Prado da Silva,<sup>2</sup> C. Royon,<sup>5</sup> A. Santoro,<sup>2</sup> M. Souza,<sup>1</sup> M.A. Strang,<sup>8</sup>  
A. Sznajder,<sup>2</sup> M. Vaz<sup>1</sup>

<sup>1</sup>*LAFEX, Centro Brasileiro de Pesquisas Físicas, Rio de Janeiro, Brazil*

<sup>2</sup>*Universidade do Estado do Rio de Janeiro, Rio de Janeiro, Brazil*

<sup>3</sup>*Instituto de Física Teórica, Universidade Estadual Paulista, São Paulo, Brazil*

<sup>4</sup>*Universidad de Los Andes, Bogotá, Colombia*

<sup>5</sup>*DAPNIA/Service de Physique des Particules, CEA, Saclay, France*

<sup>6</sup>*Moscow State University, Moscow, Russia*

<sup>7</sup>*Fermi National Accelerator Laboratory, Batavia, Illinois 60510*

<sup>8</sup>*University of Texas, Arlington, Texas 76019*

## Abstract

We present a first version of the forward proton identification using the Forward Proton Detector at DØ. We establish the characteristics of the standard proton object to be employed in the summer diffractive physics analysis. This version is mainly for use with the elastic data from the FPD stand-alone DAQ. We provide a set of standard cuts that should be used for the detection, identification and reconstruction of the particle that reaches the FPD.

---

<sup>†</sup> Instituto de Física, Universidade Federal do Rio de Janeiro, Brazil

## Contents

<b>1</b>	<b>Introduction</b>	<b>3</b>
<b>2</b>	<b>Standard Proton Identification</b>	<b>4</b>
2.1	Hit coincidence and hit confirmation . . . . .	5
<b>3</b>	<b>Offline Reconstruction</b>	<b>6</b>
3.1	Offline Reconstruction Efficiency . . . . .	7
3.2	Resolutions . . . . .	7
3.3	Geometrical and Total Acceptance of the FPD . . . . .	7
<b>4</b>	<b>Current Trigger Situation</b>	<b>13</b>
<b>5</b>	<b>Selection Cuts</b>	<b>14</b>
5.1	Elastic Particle . . . . .	14
5.2	Diffraction Particle . . . . .	15
<b>6</b>	<b>Background Rates</b>	<b>16</b>
6.1	Background . . . . .	16
<b>7</b>	<b>Calibration</b>	<b>16</b>
<b>8</b>	<b>Comparison Data-Monte Carlo</b>	<b>16</b>
<b>9</b>	<b>Triggers and Efficiencies</b>	<b>17</b>
9.1	L1 Trigger Overview . . . . .	17
<b>10</b>	<b>Proton Momentum Efficiency</b>	<b>18</b>
<b>11</b>	<b>Trigger Efficiency</b>	<b>18</b>
<b>12</b>	<b>First results for the elastic distributions</b>	<b>18</b>

# 1 Introduction

The detection of forward protons\* is primarily performed by the Forward Proton Detector (FPD), described in Ref. [1, 2]. The FPD is made up of 6 castles containing 18 Roman pots that form 9 spectrometers: 4 in the proton arm (PU, PD, PI, PO) and 5 in the anti-proton arm (AU, AD, AI, AO, DI) — See Fig. 1 and Table 1.

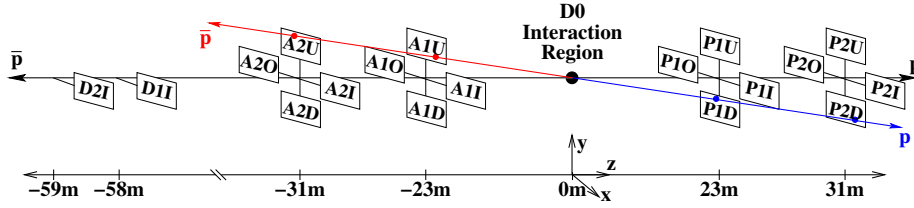


Figure 1: FPD in the Tevatron tunnel

Spec ID	Spec Name	Pots Names
1	PU	P1U + P2U
2	PD	P1D + P2D
3	PI	P1I + P2I
4	PO	P1O + P2O
5	AU	A1U + A2U
6	AD	A1D + A2D
7	AI	A1I + A2I
8	AO	A1O + A2O
9	DI	D1I + D2I

Table 1: Spectrometers

In each Roman pot there is a detector containing 3 planes ( $U$ ,  $V$ ,  $X$ ) of 0.8 mm thick square scintillating fibers. A fiber channel in each plane consists of four scintillating fibers, one on the top of the other. These channels are separated by  $1/3$  of a fiber width, with each plane having two layers of parallel fibers ( $U - U'$ ,  $V - V'$ ,  $X - X'$ ), the unprimed layer being offset by  $2/3$  of a fiber width with respect to primed ones.  $U$  and  $V$  planes are oriented at  $\pm 45^\circ$  with respect to the

\*We refer as “proton” both proton and/or antiproton



Figure 2: Detector frames

horizontal bottom of the detector, while the  $X$  plane is at  $90^\circ$ . There are 20 fibers in each layer of the  $U$  and  $V$  planes, and only 16 fibers in each of the  $X$  layers.

The 112 channels in each detector are read out by seven 16-channel multi-anode photomultipliers (MAPMT). Each detector also include a trigger scintillator read out by a fast photomultiplier.

This version “I” of the Forward Proton ID Certification document deals with the present status of our hardware setup. In this first phase of the operations, we have been using a standalone data acquisition system to collect data on proton–antiproton elastic cross section.

## 2 Standard Proton Identification

Ideally a forward proton would leave a signal in all 3 planes of a particular detector, but in some cases, due to the detector geometry or inefficiencies, we may allow 2 out of 3 planes to tag these particles. This is one of the criteria that can be used to define “loose” and “tight” quality cuts.

Other trigger elements include the FPD trigger scintillator, the Luminosity Monitor (LM), the forward veto scintillator counters, and in the particular case of diffractive events, tracking and calorimeter information. We can define at least 2 distinct objects:

- Elastic Particle (only  $p$  and  $\bar{p}$  in the event)
- Diffractive Particle ( $p + X$ ,  $\bar{p} + X$ ,  $p + \bar{p} + X$ )

After the complete integration with DØ DAQ, we will have two independent ways of finding diffractive events, either via the rapidity gap selection using the central DØ detector, the Luminosity Monitor and the veto counters, or via the tagged pro-

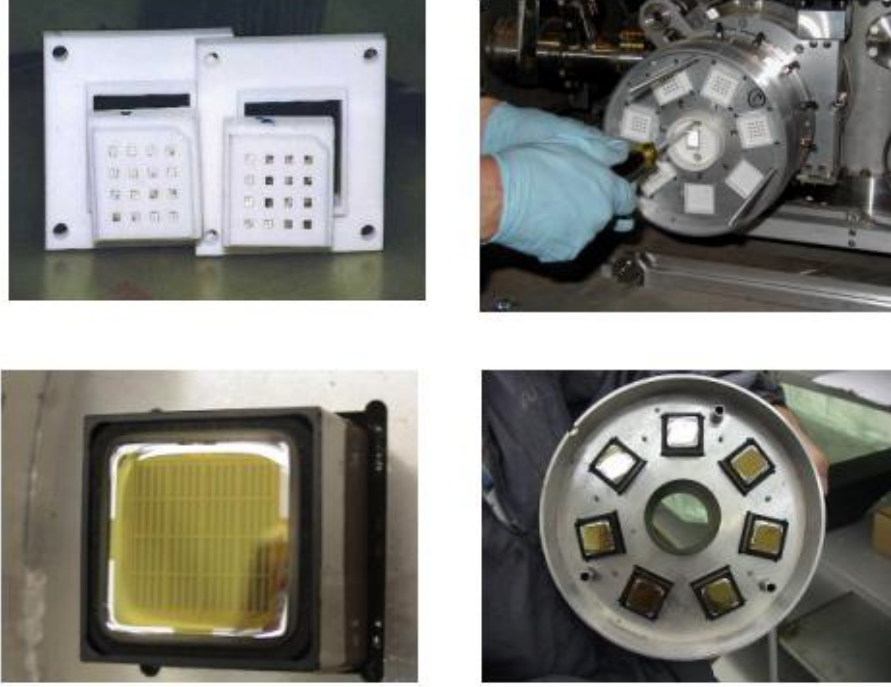


Figure 3: Detector setup

ton at the FPD, with no requirement in the  $D\emptyset$  detector. This will allow us to study rapidity gap events and gap survival probabilities.

## 2.1 Hit coincidence and hit confirmation

The hits in one detector should be compatible with the passage of a forward particle, *i.e.* with trajectories making an angle of less than  $100 \mu\text{radians}$  with the  $z$  axis. These hits are combined into segments that can comprise one hit in each layer (e.g.  $U$  and  $U'$  — see Fig. 4) or a hit in just one of the layers of this plane (e.g.  $U'$ ). This gives a total of 79 possible segments for  $U$  and  $V$  planes, and 63 for the  $X$  plane. Each segment have a width of  $0.27 \text{ mm}$ , giving a theoretical spatial resolution of  $270 \mu\text{m}/\sqrt{12} \sim 80 \mu\text{m}$ .

We define a “loose hit” in our detector as a coincidence between hit segments in two different planes of scintillating fibers. We also define a “tight hit”, for the case where there are hit segments in all three planes of fibers, in this case, the segment combination in the  $U$  and  $V$  planes should be confirmed by a signal in the  $X$  plane. This combination removes unphysical hits and can reduces the effect of noise and stray particle hits.

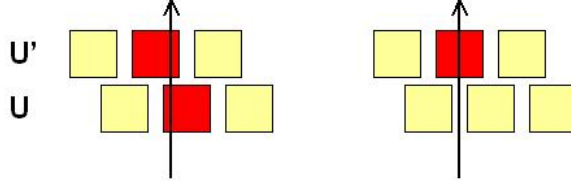


Figure 4: Hit segments

A “valid” track is defined only if there are hits (“loose” or “tight”) that match in the same arm of a given spectrometer (e.g. PD — See Table 1). Here, depending on the quality of the hits, we can define “loose” and “tight” tracks.

### 3 Offline Reconstruction

The goal of the FPD reconstruction is to determine the values of the  $\xi$  fraction of momentum carried by the Pomeron, and  $t$ , transferred squared momentum, starting from the measurements of the transverse coordinates  $(x, y)$  of the tracks in the Roman Pots of a given spectrometer stations [3, 4].

From the coordinates measured at each spectrometer we can determine the slope  $(dx/dz, dy/dz) \equiv (\theta_x, \theta_y)$  and construct the vector,

$$\Omega = (x, y, \theta_x, \theta_y)$$

The Tevatron lattice parameters matrix,  $T_{ij}$ , can be used to propagate  $\Omega$ , from the Roman Pot (RP) to the Interaction Point (IP), i.e.,

$$\Omega_i^{\text{IP}} = T_{ij}(\xi) \Omega_j^{\text{RP}}$$

and determine the  $(x, y)$  values at  $z = 0$ . The diffracted angle is given by  $\theta = (\theta_x^2 + \theta_y^2)^{1/2}$ .

Assuming that the initial proton loses a fraction  $\xi$  of its momentum  $p_b$ , we can write for the diffracted proton ( $p_f$ ),

$$p_f = x.p_b = (1 - \xi)p_b$$

or  $\xi = (p_b - p_f)/p_b$ . The squared transfer momentum  $t$  is given by,

$$t = (p_f - p_b)^2 \simeq -(1 - \xi) E_b^2 \theta^2$$

for small  $\theta$  and  $E_b \gg M_p$ .

From the geometrical coverage of the FPD detector in the present configuration, which uses only vertical detectors, we have:

$$0.6 < |t| < 2.0 \text{ GeV}^2, \text{ and } 0 < \xi < 0.1$$

Therefore we can establish the  $\eta = -\log(\tan \theta/2)$  coverage of the detector as,

$$7.2 < \eta < 7.8$$

### 3.1 Offline Reconstruction Efficiency

### 3.2 Resolutions

In order to determine the  $\xi$  and  $t$  resolutions, a Monte Carlo algorithm was developed. A forward proton with known initial values of  $\xi_0$  and  $t_0$ , is sent from the interaction point ( $z = 0$ ) position to the pot locations. In this way we can determine the struck fibers [3, 4]. The algorithm first transforms fibers into segments, and segments into  $(x, y)$  transverse coordinates at pot locations ( $z_{\text{pots}}$ ). This allows the determination the slopes  $(\theta_x, \theta_y)$  at the pot closest to the interaction point. An iteration procedure is then launched by the algorithm to find the best set of  $(\xi_{\text{reco}}, t_{\text{reco}})$  that corresponds to the  $(x, y)$  transverse coordinates at Pot locations ( $z_{\text{pots}}$ ) [3]. The resolutions  $\Delta\xi = \xi_{\text{reco}} - \xi_0$  and  $\Delta t = t_{\text{reco}} - t_0$  obtained for the spectrometers PU, PI, and DI are shown in Fig. 5 to 7. Due to the Tevatron lattice the results for vertical spectrometers on the P side are identical to the horizontal on the A side.

### 3.3 Geometrical and Total Acceptance of the FPD

The Forward Proton Detector system was built with the purpose of measuring in detail all diffractive channels that account for nearly 40% of the total cross section at the Tevatron's  $\sqrt{s}$  energy. We can parametrize the single diffractive cross section as,

$$\frac{d\sigma}{dt} \sim A \exp[-b(\xi)|t|]$$

where

$$b = \frac{d}{dt} \ln \frac{d\sigma}{dt} \Big|_{t=0}$$

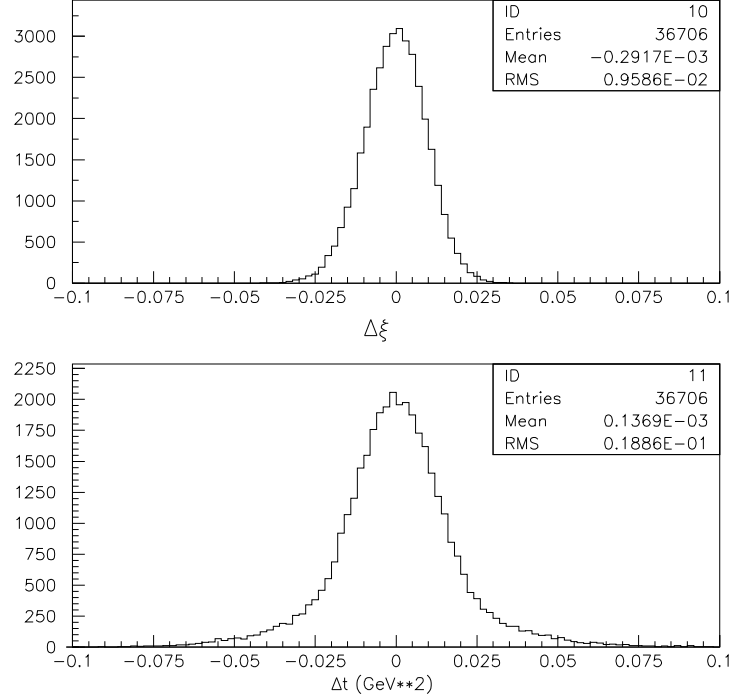


Figure 5: Simulated  $\Delta\xi$  and  $\Delta t$  resolutions for protons detected in the PU spectrometer. The resolutions were obtained using a MC algorithm that sends protons from the Interaction Position to pot locations with momentum losses  $\xi_0$  and squared transfer momentum  $t_0$  for  $\xi = 0$  (elastic process) and  $0 \leq t \leq 5 \text{ GeV}^2$ , respectively. The reconstruction algorithm is then used to transform the channel hits in transverse positions  $(x, y)$  at each pot locations and finds the values of  $\xi_{\text{reco}}$  and  $t_{\text{reco}}$  of each event, which allows to obtain the resolutions  $\Delta\xi = \xi_{\text{reco}} - \xi_0$  and  $\Delta t = t_{\text{reco}} - t$ .



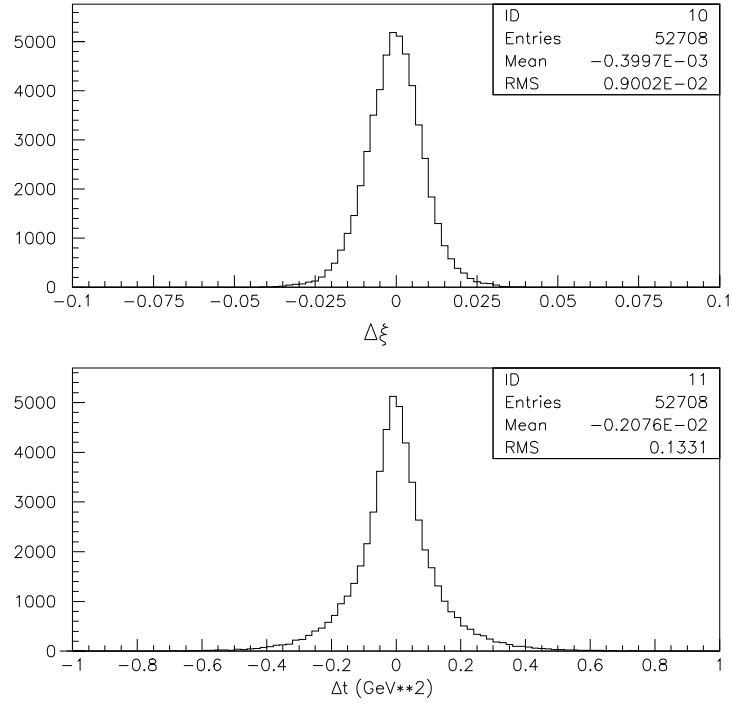


Figure 6: The **same** as Figure 5, for protons detected in the horizontal **PI** Quadrupole spectrometers.

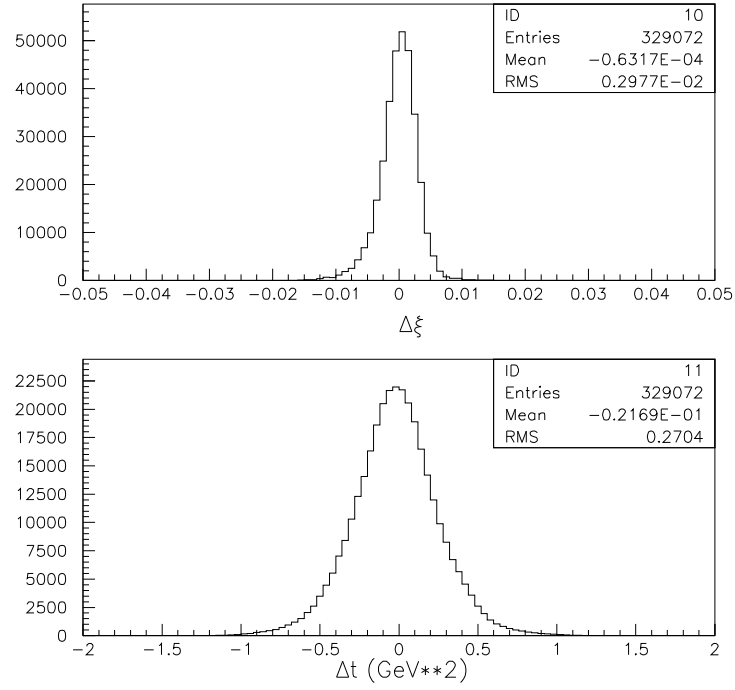


Figure 7: The **same** as Figure 5, for protons detected in the horizontal **DI** Dipole spectrometers.

The differential acceptance for a detector with cylindrical symmetry is a normalized function of  $t$  and  $\phi$  given by,

$$\mathcal{A}(\xi, t, \phi) dt d\phi = \frac{1}{\sigma(\xi)} \frac{d\sigma}{dt} dt dA_\phi$$

where  $dA_\phi = d\phi/2\pi$  is the geometrical acceptance. Since the cross sections for these channels depend both on the geometrical and angular acceptances, we performed a study taking into account both acceptances with the tracking algorithm [5]. The results obtained within this study are shown in Figs. 8 and 9 for the geometrical acceptance at dipoles and quadrupole spectrometers. In Figs. 10 and 11 we present the integrated acceptance for horizontal and vertical planes of the quadrupole spectrometer. The total quadrupole acceptance is shown in Fig. 12 for quadrupoles and in Fig. 13 for the dipole pots. As we have pointed out before (pag. 7), due to the lattice asymmetry for  $p$  and  $\bar{p}$  beams the vertical acceptance in the proton side is equivalent to the horizontal acceptance in the antiproton side and vice-versa.

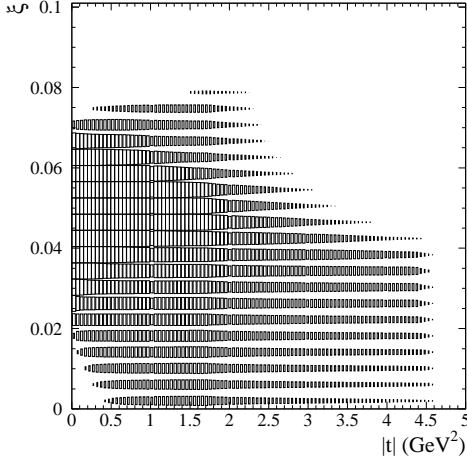


Figure 8:  
Geometric acceptance in bins of  $\xi$  and  $|t|$  for the dipole spectrometer, with the detector at  $8\sigma$  displacement. The acceptance in each bin is proportional to the size of the box, with the largest box representing 100% acceptance.

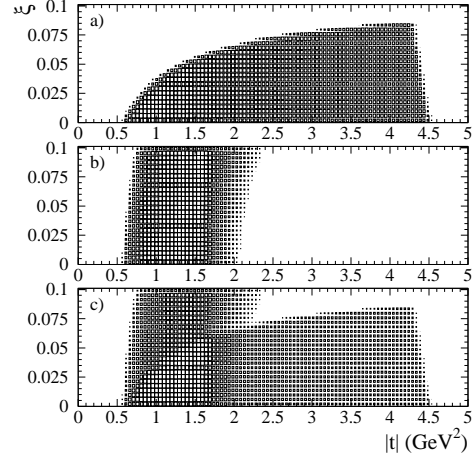


Figure 9:  
Geometric acceptance for quadrupoles (proton side) at  $8\sigma$  displacement: (a) horizontal: (b) vertical and (c) sum of both pots in bins of  $\xi$  and  $|t|$ . The size of the box is proportional to the value acceptance in that range of the parameters (see Fig. 8 caption)

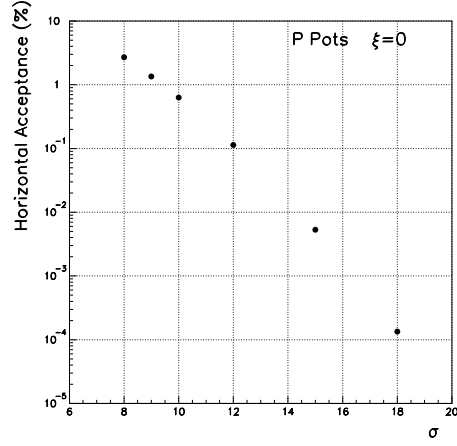


Figure : 10  
Acceptance (in %) integrated on  $\phi$  and  $|t|$   
for  $\xi = 0$  at different horizontal pot positons.

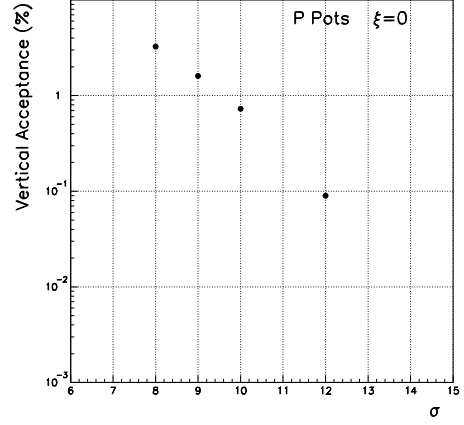


Figure 11:  
Acceptance (in %) integrated on  $\phi$  and  $|t|$   
for  $\xi = 0$  at different vertical pot positons.

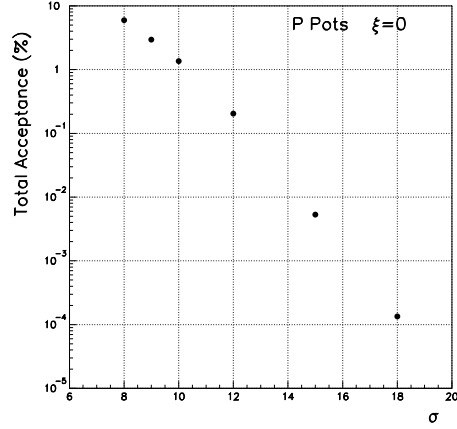


Figure 12:  
Total (horizontal plus vertical) acceptance  
(in %) for  $\xi = 0$  at different pot positons.

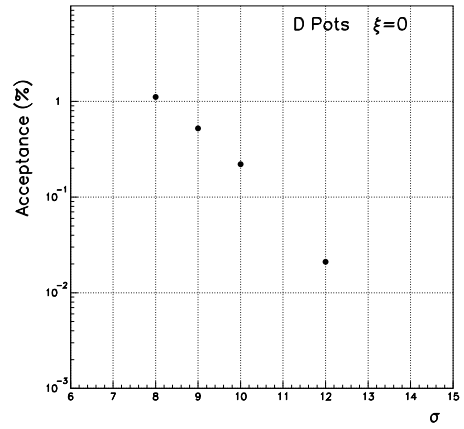


Figure 13:  
Total dipole acceptance (in %) for  
 $\xi = 0$  at different pot positons.

## 4 Current Trigger Situation

The present DAQ system for the FPD is based on a stand-alone setup of NIM and CAMAC modules. The implemented trigger is based on coincidences of trigger scintillator along with vetoes on luminosity counters and veto counters [8].

The DØ interaction marker clock is used as reference to generate two clocks: one for the incoming particles (early clock) and the other for the outgoing particles (in-time clock). With the early and the in-time signals we can build the trigger logic to select the elastic events with the NIM modules. If the event passes the requirements, it will open the CAMAC gate to accept the signals coming from the MAPMT's.

The trigger logic for the elastic events are based in the coincidence of the in-time particles at each opposite diagonal spectrometer. Because we have instrumented only the vertical plane we can only detect two possible elastic branches given by the coincidence of the in-time particles passing through the detectors A1U.A2U.P1D.P2D and A1D.A2D.P1U.P2U

In order to clean up the events from halo background we create a Veto term (negated) in coincidence with the in-time signals. This Veto term is formed with an OR of any Early particles OR any signal in the luminosity monitors OR any activity in the Veto counters.

In summary the elastic trigger logic is given by

$$\begin{aligned} & A1U.A2U.P1D.P2D.\overline{VETO} \\ & A1D.A2D.P1U.P2U.\overline{VETO} \end{aligned}$$

where the VETO term is given by

$$\begin{aligned} VETO = & (EA1U + EA2U + EP1D + EP2D) + (LMN + LMS) \\ & + [(V1N.V2N) + (V1S.V2S)] \end{aligned}$$

The diffractive triggers (one Loose and one Tight) are constructed requiring a coincidence of in-time particles in one spectrometer, for example the

$$P1D.P2D.\overline{VETO}$$

where the veto is performed with an OR of Early diagonal opposite particles OR any signal in the DØLM AND Veto Counters of the same hemisphere of the outgoing tagged particle. For example for the PD spectrometer the Loose trigger will be [9]

$$LOOSE = P1D.P2D.\overline{VETO}$$

with

$$VETO = EP1D + EP2D + LMS + (V1S.V2S)$$

while for the Tight condition the trigger condition is

$$TIGHT = P1D.P2D.[LMN + (V1N.V2N)].\overline{VETO}$$

where

$$\begin{aligned} VETO &= EP1D + EP2D + LMS + (V1S.V2S) + (P1U.P2U) \\ &+ (A1U.A2U) + (A1D.A2D) \end{aligned}$$

## 5 Selection Cuts

As stated above, our goal is to measure elastic and diffractive processes that account for nearly 40% of the total cross section for  $p + \bar{p}$  reaction at the Tevatron. Since there are both soft (*e.g.* elastic and low mass diffractive) and hard (*e.g.* jets) processes, specific selection cuts have to be used to tag these objects, which will lead to different tagging efficiencies. Finally, care must be taken to eliminate any background signal that can mimic the physical process.

### 5.1 Elastic Particle

For the elastic process, defined by  $\xi = 0$ , both particles must be detected by diagonally opposite spectrometers, as for example  $\bar{p}$  in AU and  $p$  in PD spectrometers. Furthermore, no activity would be expected in any other DØ sub-detector. A typical exclusive trigger requires no activity in any LM counters, and in any of the forward veto counters ( $5.2 \leq |\eta| \leq 5.9$ ). We can use also the timing information from our trigger scintillator to verify that the forward particles originate from the interaction point. In this way we are able to measure the differential distribution  $dN/dt$  as a function of the squared transferred momentum  $t$ , and consequently, determine the differential cross section. Since acceptance studies show that a large range of  $t$ -values can be measured with the FPD system, the differential elastic cross-section can be studied in great detail.

Measuring  $d\sigma/dt$  at small  $t$  is crucial in order to extrapolate the measured cross-section to  $t = 0$ , *i.e.* the optical point, and to obtain the total cross-section by applying the optical theorem. This will require special beam conditions like low emittance and luminosity to get the detectors close to the beam and avoid multiple interactions.

After collecting the elastic data sample we apply the following cuts offline:

- We apply a 50 ADC count discrimination threshold to all channels to determine if a channel is on or off;
- We require that each plane ( $U, U', X, X', V, V'$ ) have 0 or 1 fibers turned on in both detectors for the same event;
- For these events, we require for each frame (i.e.,  $U/U', X/X', V/V'$ ) that we have 1/0, 0/1 or 1/1 fibers turned on in both detectors;
- Finally, we require that the fibers reconstruct into a valid segment;

Around 2% of the events pass these cuts. These events are then passed through the following tracking reconstruction cuts:

- Fibers in each frame are required to match a valid segment in that specific frame;
- Valid  $U/U'$  and  $V/V'$  segments must be aligned to a  $X/X'$  segment such that transverse  $x$  position, which can be independently determined either from  $U/U'$  and  $V/V'$  or from  $X/X'$ , has values that not differ more than 0.5 mm;
- We consider valid tracks the ones with transverse  $(x, y)$  positions at both detectors of a given spectrometer that are reconstructed to the interaction point. We also require that the track have a trajectory that stays inside the beam pipe (35 mm) and the separator aperture (25 mm).

Around 80% of the events survives this second set of tracking selection cuts.

## 5.2 Diffractive Particle

In the case of the diffractive processes, we can use some of the tools of the elastic process to reduce the background, for instance, the timing information for the particle and veto on the LM and veto counters on the outgoing particle arm. The studies on the diffractive particle can be made as a function of both  $\xi$  and  $t$  variables, by means of the double differential cross section  $d^2\sigma/d\xi dt$ . The FPD system will also allow the measurement of double Pomeron exchange by tagging both  $p$  and  $\bar{p}$  in the spectrometers and requiring the presence of activity in the DØ central detector.

## 6 Background Rates

### 6.1 Background

There are different types of false track backgrounds that must be considered in forward proton identification:

- **Halo track:** A halo track, caused by off axis particles, can generate hits in a spectrometer that are indistinguishable from a forward proton that originates from the interaction. This “fake” background can be rejected using timing information from the diagonally opposite spectrometer, as the halo particle will pass through 77–103 ns before the interaction.
- **Spray from the beam loss:** Protons and antiprotons lost from the main bunches can interact producing multiple hits in detectors resulting in false tracks. This problem can be reduced using multiplicity cuts on the number of valid segments.
- **Multiple interactions:** Several interaction per bunch crossing can be tackled using the information coming from the Luminosity Monitor, Silicon Vertex detector and Calorimeter, to keep their rates small. In any case, at the current luminosity, we do not expect that multiple interactions could be a important problem.

Other sources of background, like detector and electronic noise can also be controlled asking for “tight” definition of hits in the detectors, however this will result in a small efficiency loss.

## 7 Calibration

Elastic data will provide good calibration for the FPD system. Indeed, in elastic data, the in-time rate at one spectrometer arm at one side, must match the rate at opposite spectrometer at the other arm, as for instance in AD-PU case. By comparing rates at opposite arms, a good calibration can be achieved for pot positioning. Furthermore, using the reconstruction algorithm to determine the values of  $\xi$  and  $t$  for elastic events at the interaction point, will also aid in calibration.

## 8 Comparison Data-Monte Carlo

Monte Carlo simulations of diffractive events are of great importance in the study of diffractive channels to be performed by the Forward Proton Detector



group. In addition to the toy Monte Carlo used to study FPD performance, simulations are needed to study diffractive and non-diffractive physics processes. The current codes (POMPYT, PHOJET, POMWIG, etc) for diffractive interactions are being used as well as the non-diffractive algorithms (PYTHIA, ISAJET, etc).

## 9 Triggers and Efficiencies

### 9.1 L1 Trigger Overview

The Forward Proton Detector, after integration with DØ, will send to the **L1 Trigger Framework** and **L3 Filtering System** information about hits from its 18 Roman Pots [6]. Each Roman Pot has a 112 channel position (tracking) detector that generate light pulses in the scintillating fibers. This information is converted to electric current pulses in a 16 channel multiple anode photo multiplier tube (MAPMT).

For the L1 we use standard DØ CFT trigger electronics, Analog Front End board (AFE) and Digital Front End board (DFE) to make a trigger decision. In the AFE, Multi chip modules (MCM) receive the amplified signal from the MAPMTs, discriminate and latch them, and also convert pulse amplitude to digital form. The discriminated signals from the AFE are sent through LVDS links to Digital Front End boards (DFE) where the decision of keeping or not the event is made.

The DFE uses FPGA's to match the pattern of the hit fibers with that of valid tracks to determine  $\xi$  and  $t$  bins of valid tracks. It also performs a multiplicity cut to remove background from spray. It then sends valid track information to the L1 Trigger Manager board, which also receives timing information from the LM and FPD Luminosity Monitor boards. The signals generated by the Trigger Manager board are sent to the Trigger Framework. The DFE also continuously sends information about their data processing to Level 3.

Some dedicated triggers will be required [7]:

- **Diffractive Jet Production** will combine a low  $E_T$  cluster with a track in  $p$  or  $\bar{p}$  spectrometer;
- **Double Pomeron exchange** will require tracks in both  $p$  and  $\bar{p}$  spectrometer and a low  $E_T$  cluster for the hard double Pomeron exchange case;
- **Inclusive single diffraction** will be necessary to study the soft diffraction and the ratios of diffractive jet production to inclusive diffraction;
- **Elastic scattering** requires tracks in diagonally opposite quadrupole spectrometers and can be used also for alignment purposes and luminosity monitoring

In order to minimize the bandwidth for these dedicated triggers it is important to implement cuts on the kinematical variables  $\xi$  and  $t$  at the Level 1.

When the AFE/DFE boards are available and our DAQ is completely integrated in the whole DØ system we should implement the “AND–OR” Terms similar to those of the Global Trigger List.

## 10 Proton Momentum Efficiency

Information about the proton momentum efficiency will be provided soon.

## 11 Trigger Efficiency

Measuring efficiencies for the trigger scintillator can be done by forming a A1U.A2U.P2D trigger for example and looking at how often P1D trigger scintillator is ON when P1D fibers are ON. Efficiency should be very high.

This procedure can be repeated for other trigger scintillator in a similar way. This should be checked for good elastic events versus all events, because background events which spray the scintillators might have higher efficiency.

We should also study trigger efficiencies by adding the vetoes one by one and measuring the rate of good elastic events to see the efficiency of each veto (vetoes should only reject background). Until we have DFE boards the proton part of the trigger will be based solely on the terms we are using now.

In parallel we should be studying multiplicity cuts (offline) to reject background spray event. We will then implement these cuts online in DFE and again use elastic rate with and without cuts to examine efficiency.

This same procedure will be repeated when we employ triggers that cut on  $\xi$  and  $t$  at Level 1, using the DFE boards.

## 12 First results for the elastic distributions

We present here our first physical distributions using the elastic trigger described above. Figure 14 shows the scatter plot of the nominal  $x$  positions of the proton track in two different detectors of the spectrometer (P1D and P2D). The same scatter plot for the nominal  $y$  position of the track is presented in Fig. 15. This distributions are compared with the result of the Monte Carlo simulation. We should notice that the width of the data distribution is 1.6 larger than the width of the ideal MC distribution that does not take into account the smearing of the detector. The offset of the correlation indicate a misalignment of the detectors which

present a relative displacement of 3 mm in the  $x$  and 1 mm in the  $y$  direction.

The corresponding  $\xi$  distribution for this situation is shown in Fig. 16 (a). We notice that the distribution is not peaking at  $\xi = 0$ . That should be the case since we are considering only elastic events. However, after the misalignment is corrected by shifting the relative pot position, the  $\xi$  distribution becomes well behaved as can be seen in Fig. 16(b), where the tail comes from the contamination from diffractive events. The same behavior can be seen in the fitted result (Fig. 16(c)), where the Gaussian fit took into account the reconstructed  $\xi$  in the range  $-0.05 \leq \xi \leq 0.05$ .

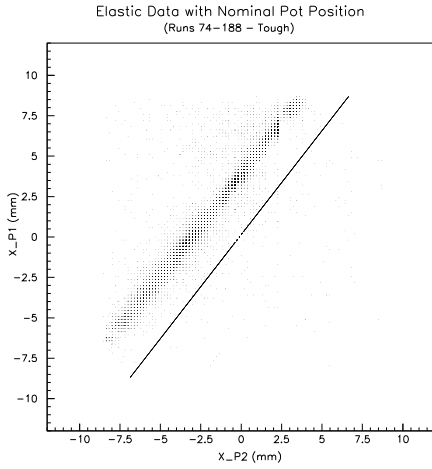


Figure 14:  
Elastic data and Monte Carlo simulation for  
the nominal  $x$  position of the hit

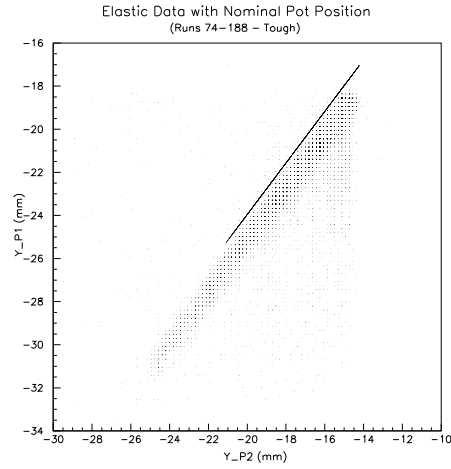


Figure 15:  
The same as Fig. 14 for the nominal  $y$   
position.

We also present here in Fig. Fig. 16(d) the  $t$ -distribution for the same sample of elastic events. This distribution should depend only on the angular acceptance of the detectors and it is in agreement with our Monte Carlo result. The structures present in this figure could be related to dead channels or to the contamination of the sample from diffractive events.

Our results for diffractive events is going to presented elsewhere [10].

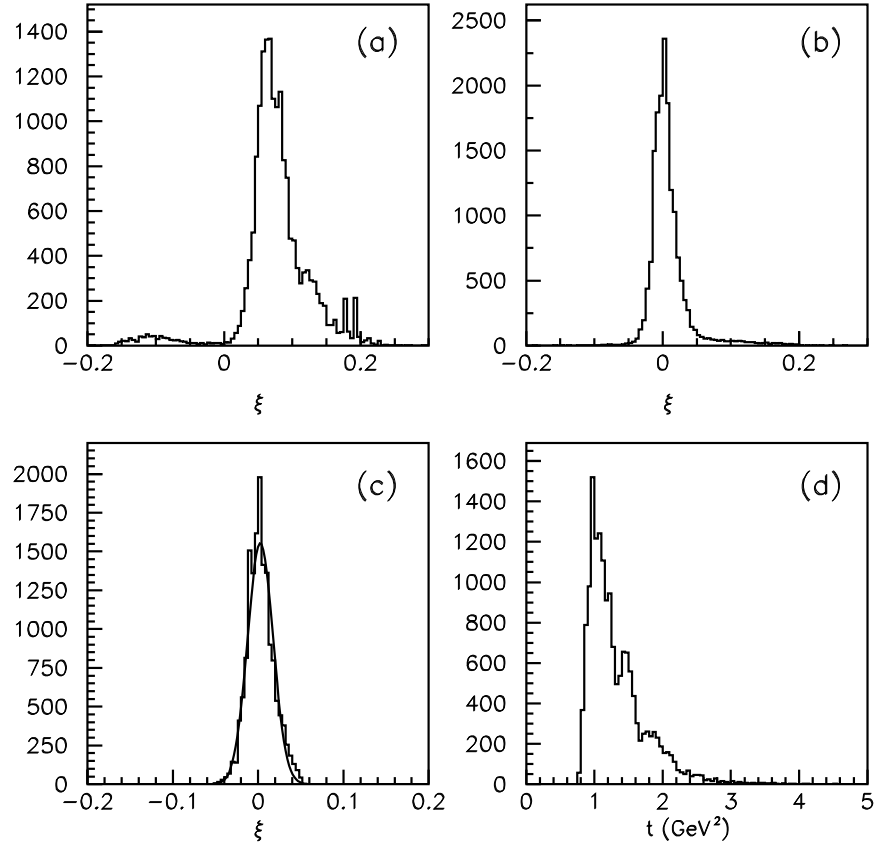


Figure 16: (a)  $\xi$  distribution before the alignment; (b)  $\xi$  distribution after the alignment; (c) fitted  $\xi$  distribution; (d)  $t$  distribution.



## References

- [1] A. Brandt *et al.*, “A Forward Proton Detector at DØ”, FERMILAB-Pub-97/377
- [2] See also the Forward Proton Detector webpage at:  
<http://www-d0.fnal.gov/fpd/Links/links.html>
- [3] J. Barreto and A. Drozdhin, “Reconstructing Track Trajectories for the FPD”, DØ Note Nø 3788, November 2000.
- [4] J. Barreto, “Detector Identification in the FPD System” DØ Note Nø 3789, November 2000.
- [5] J. Barreto and J. Montanha, “Acceptance Studies for FPD” DØ Note Nø 3790, November 2000.
- [6] M. Vaz, “Forward Proton Detector L1 Trigger Electronics”,  
<http://d0br1.lafex.cbpf.br/%7Emario/FPD/FPDTL1.htm>
- [7] A. Brandt, Triggering with the Forward Proton Detector,  
[http://www-d0.fnal.gov/~brandta/fpg/d0\\_private/trigger/fpd\\_trigger.ps](http://www-d0.fnal.gov/~brandta/fpg/d0_private/trigger/fpd_trigger.ps)
- [8] C. Avila, “FPD Beam Test DAQ”,  
<http://www-d0.fnal.gov/~avila/fpddaqa.htm>
- [9] P. Hanlet, “Logic diagrams for FPD triggers”,  
<http://www-d0.fnal.gov/~hanlet/>
- [10] G.A. Alves, *et al.*, “Forward Proton ID Certification II: Diffractive Process and Standalone DAQ”, in preparation.